Hyperon and Charged Kaon Pair Production Close to Threshold

M. Wolke[†], H.-H. Adam[*], J.T. Balewski[†,||,¶], A. Budzanowski[||], C. Goodman[¶], D. Grzonka[†], L. Jarczyk[§], M. Jochmann[‡], A. Khoukaz[*], K. Kilian[†], M. Köhler[‡], P. Kowina[††], T. Lister[*], P. Moskal[†,§], N. Lang[*], W. Oelert[†], C. Quentmeier[*], R. Santo[*], G. Schepers[*,†], U. Seddik[**], T. Sefzick[†], S. Sewerin[†], M. Siemaszko[††], J. Smyrski[§], A. Strzałkowski[§], P. Wüstner[‡], W. Zipper[††]

[†] *Institut für Kernphysik, Forschungszentrum Jülich, D–52425 Jülich, Germany*
[*] *Institut für Kernphysik, Westfälische Wilhelms–Universität, D–48149 Münster, Germany*
[||] *Institute of Nuclear Physics, PL–31–342 Cracow, Poland*
[¶] *Indiana University Cooler Facility, Bloomington, IN 47405, USA*
[§] *Institute of Physics, Jagellonian University, PL–30–059 Cracow, Poland*
[‡] *Zentrallabor für Elektronik, Forschungszentrum Jülich, D–52425 Jülich, Germany*
[††] *Institute of Physics, University of Silesia, PL–40–007 Katowice, Poland*
[**] *Egyptian Atomic Energy Authority, 13759 Cairo, Egypt*

Abstract. Close–to–threshold data on the elementary kaon and antikaon production channels in the proton–proton interaction have been taken using the COSY–11 installation at the cooler synchrotron COSY Jülich.

The experimental technique applied at the internal COSY–11 facility — designed for meson production studies at small excess energies — is outlined. The threshold excitation functions for the kaon–hyperon production via the reactions $pp \to pK^+\Lambda$ and $pp \to pK^+\Sigma^0$ are presented. The magnitude of the production amplitudes is compared at equal excess energies and physical implications of the observed Σ^0 suppression in the threshold region are discussed. In addition, within a Dalitz plot analysis the spin–averaged S–wave scattering parameters could be extracted for the Λ–p channel.

With the possibility of detecting all final state particles the elementary antikaon production in the reaction $pp \to ppK^+K^-$ has been investigated. Results on the exclusive total cross section fix the scale of the strangeness dissociation into two kaons.

INTRODUCTION

The associated strangeness production in proton–proton collisions close to threshold provides an elucidative probe for studying both the structure of the nucleon and the baryon–baryon interaction.

As reaction dynamics are expected to depend on the strangeness content in the initial state, strangeness production directly addresses the strangeness content of the nucleon on the sea quark level. The strange–antistrange quark pair creation at threshold requires high momentum transfers between the colliding nucleons. Consequently, the short range part of the nucleon–nucleon interaction is probed.

Close to the reaction threshold only few partial waves contribute, simplifying the theoretical interpretation of the data. With vanishing relative momenta in the exit channel, from extended interaction times the experimental observables are influenced by strong final state interaction effects. In turn, the elastic interaction in the final state may be used to extract low energy scattering parameters.

Both the strangeness dissociation into a kaon–hyperon and a kaon–antikaon system have been studied at the COSY–11 facility in the nucleon–nucleon collision. Close–to–threshold cross section values of elementary kaon and antikaon production are an essential input for transport model calculations to describe the strangeness production in heavy ion collisions.

EXPERIMENTAL TECHNIQUE

The internal COSY–11 facility at the proton synchrotron and storage ring COSY Jülich [1] has been designed for threshold meson production studies. ¿From the experimental point of view, due to small transverse momenta close to threshold, ejectiles are limited to a narrow forward cone in the laboratory. Thus, the concept of an internal magnetic spectrometer with 4π geometrical acceptance at threshold is attainable with a comparatively small detector setup.

A cluster target [2] is installed in front of a regular C–shaped COSY dipole which both separates reaction products from the circulating beam and analyzes their momenta (fig. 1). Two sets of drift chamber stacks (D1,D2 in fig. 1) allow to measure the direction of positively charged reaction products, which are diverted towards the inside of the storage ring. Particle momenta are reconstructed from tracing back of the trajectories through the well known dipole field towards the target position. A particle identification is achieved by combining the momentum information with time–of–flight measurements.

For the ppK^+K^- and pK^+Y final states — where Y denotes a hyperon — start and stop timings for the proton identification are generated by two scintillator arrangements S1/S2 and S3 placed with a distance of 9.1 m. Due to their short lifetime for the identification of kaons an indirect time–of–flight measurement is used: Tracing back proton trajectories towards the target position intrinsically determines the time of the event at the target as a start signal, the stop timing being provided by the "start" scintillator hodoscope S1.

Negatively charged particles, which are deflected towards the yoke of the dipole, are detected by a dedicated part of the detection system consisting of a scintillator and a high granularity array of silicon pad detectors (Si_{dip}), both mounted inside the dipole gap. Short–lived neutral mesons or baryons are identified us-

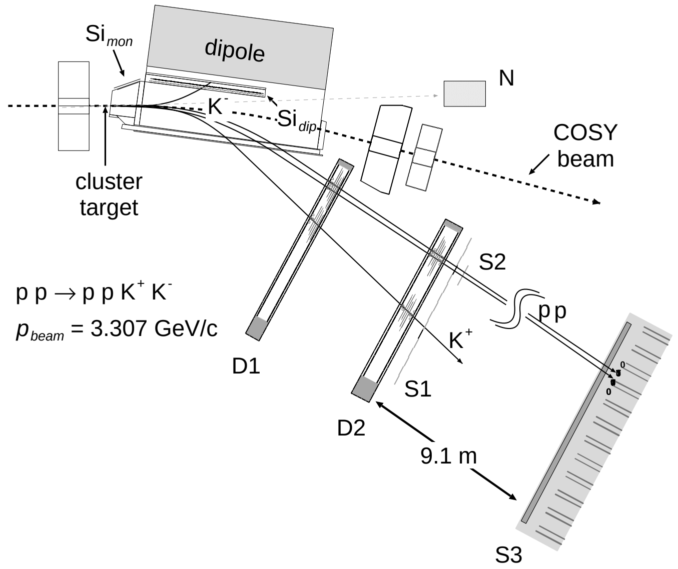

FIGURE 1. Schematic view of the internal COSY–11 installation and Monte Carlo generated particle tracks for the reaction $pp \to ppK^+K^-$.

ing the missing mass technique with the complete four–momentum information of positively charged ejectiles. The detection system is described in more detail in [3].

As an absolute normalization proton–proton elastic scattering is recorded simultaneously during data taking. Measured differential elastic counting rates are related to high precision cross section data available in the COSY energy range from the results of the EDDA collaboration [4]. Considering the integrated luminosity and the overall acceptance, i.e. both geometrical coverage and detector efficiencies studied in Monte Carlo simulations, total cross section values are derived from the observed counting rates. At present, typical luminosities at COSY–11 are in the range of $2 - 4 \times 10^{30}\,\mathrm{cm^{-2}\,s^{-1}}$.

HYPERON PRODUCTION IN PROTON–PROTON COLLISIONS

Final State Identification

For events with an identified proton in the final state the invariant mass of a second charged particle — determined from the indirect time–of–flight method — is plotted versus the missing mass with respect to the assumed (pK^+)–subsystem at an excess energy of 12.9 MeV above the Σ^0 threshold in figure 2. Enhancements at both the Λ and the Σ^0 mass are clearly visible within the invariant mass resolution for the charged kaon mass. Kaon signals at missing mass values between the hyperon masses are explained by the misinterpretation of protons originating from the

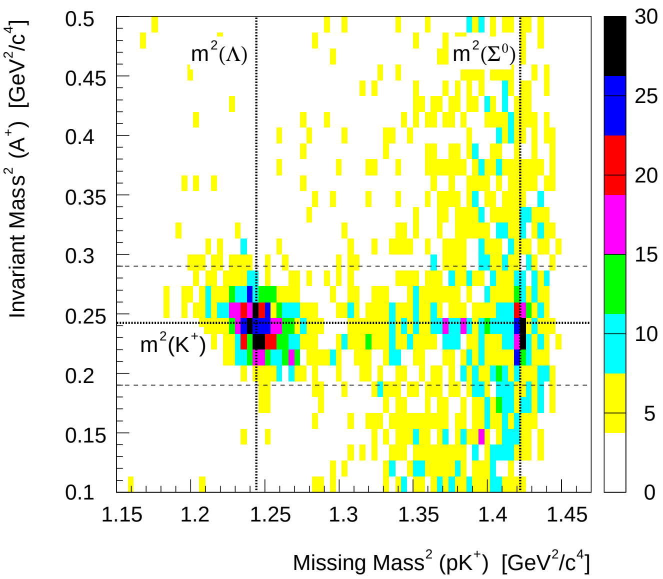

FIGURE 2. Invariant mass squared of a second charged particle in addition to an identified proton versus the missing mass squared of the assumed (pK^+) subsystem at an excess energy of 12.9 MeV with respect to the Σ^0 threshold. The range of identified kaons is limited by a cut equivalent to three standard deviations of the K^+ invariant mass distribution.

hyperon decay as protons from the primary reaction. Events outside the indicated range of the kaon mass distribution are reproduced in Monte Carlo simulations by scattering of beam particles on the rest gas or secondary reactions of elastically scattered protons in the beam pipe, i.e. by events not originating from the target. Thus, background contributions to the missing mass spectrum — the projection of events within the kaon mass resolution onto the missing mass axis in figure 3a — can be derived from equivalent projections outside the range of identified kaons (for details see [7]).

The missing mass distribution after background subtraction is depicted in figure 3b. A missing mass resolution of about $1\,\mathrm{MeV/c^2}$ is obtained at an excess energy of 12.9 MeV with respect to the $(pK^+\Sigma^0)$ threshold. The broadening of the Λ peak is understood as a kinematical effect as close to threshold the missing mass resolution approximately scales with the square root of the excess energy.

The $pp \to pK^+\Lambda/\Sigma^0$ Total Cross Section

The reactions $pp \to pK^+\Lambda$ and $pp \to pK^+\Sigma^0$ have been measured at equal excess energies up to 13 MeV at the COSY–11 installation [5–7], no further data are available in this threshold energy range.

For both hyperon production channels the energy dependence of the total cross section is much better described by a phase space behaviour modified by the (pY)

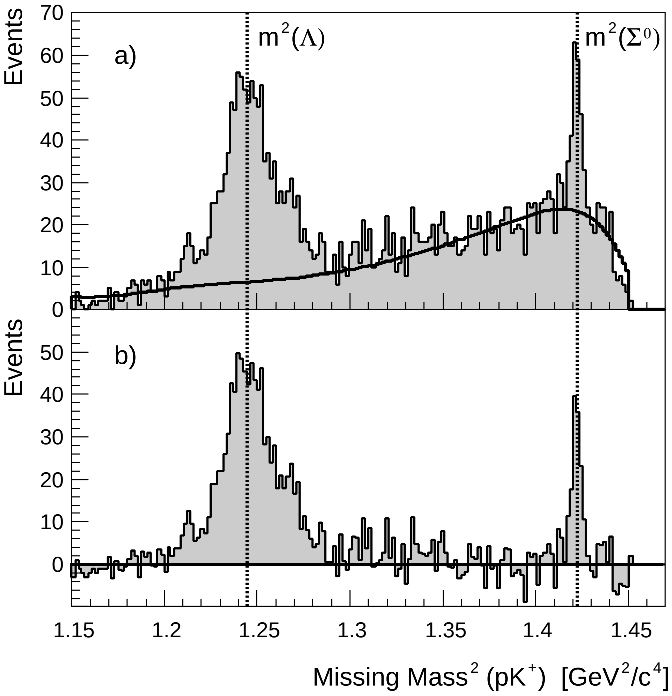

FIGURE 3. Missing mass squared with respect to the (pK^+) subsystem at an excess energy of 12.9 MeV above the Σ^0 threshold before (a) and after (b) subtraction of background (solid line).

final state interaction [8] than by a pure phase space calculation (fig. 4).

The most striking feature of the data, however, is the observed Σ^0 suppression in the close–to–threshold energy range with

$$\frac{\sigma\left(\mathrm{pp} \to \mathrm{pK}^+\Lambda\right)}{\sigma\left(\mathrm{pp} \to \mathrm{pK}^+\Sigma^0\right)} = 28\,^{+6}_{-9}, \tag{1}$$

whereas at excess energies $\geq 300\,\mathrm{MeV}$ this ratio is known to be about 2.5 [9]. The large production ratio can be discussed qualitatively against the background of a description of possible production mechanisms within the framework of the meson exchange picture:

¿From π–exchange, relating the production in nucleon–nucleon scattering to $\pi\mathrm{p} \to \mathrm{K}\Lambda\,(\Sigma)$ data [10], a cross section ratio of ≈ 0.4 underestimates the experimental results by about two orders of magnitude. Considering K–exchange the ratio in proton–proton collisions is essentially given by the ratio of coupling constants $g^2_{\mathrm{N}\Lambda\mathrm{K}}/g^2_{\mathrm{N}\Sigma\mathrm{K}}$. Despite the existing uncertainty in the literature for the coupling, the choice of the SU(6) prediction [11] results in a cross section ratio of 27 in good agreement with the data although neglecting both initial and final state interactions. Inclusive measurements of K^+ production at higher excess energies ($\mathrm{Q} \approx 170\,\mathrm{MeV}$) obtained at SPES 4 [12] show enhancements at both the Λp and ΣN thresholds of similar strength. Obviously, both the SATURNE data and the

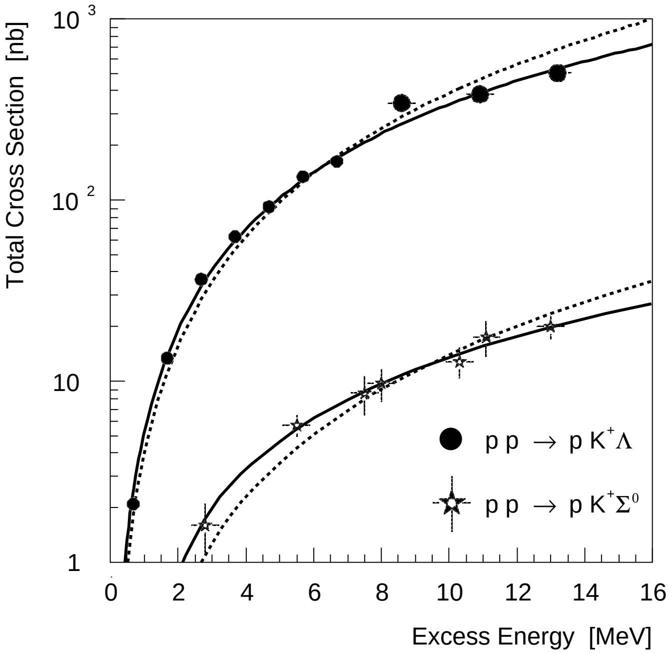

FIGURE 4. Data on the total cross section for the reactions pp $\rightarrow$ p$K^+\Lambda$ and pp $\rightarrow$ p$K^+\Sigma^0$ obtained at COSY–11 [5–7]. The statistical error is included or is smaller than the symbol size. Horizontal error bars denote the uncertainty of the excess energy. The energy dependence is much better described by a phase space behaviour modified by the proton–hyperon final state interaction (solid line [8]) than by a pure phase space calculation (dashed line).

depletion of the Σ^0 signal close to threshold observed at COSY–11 might be explained by a strong final state conversion $\Sigma N \rightarrow \Lambda p$, an effect known for example from K^- absorption on deuterium [13]. In turn, the final state conversion implies an initially larger Σ yield compared to the SU(6) prediction.

First theoretical investigations within the framework of the Jülich meson exchange model [14] taking into account both π– and K–exchange and rigorously treating the final state interaction disfavour a final state conversion as the origin of the observed large production cross section ratio. While Λ production is dominated by kaon exchange, both pion and kaon exchange are found to contribute in case of Σ production with similar strength and a destructive interference of these amplitudes is concluded to be one possible explanation of the Σ^0 suppression. It should be noted that contributions from direct production and heavy meson exchange, i.e. ρ and K^* exchange, have so far been neglected but might influence the Λ/Σ^0 production ratio [15–17].

Low Energy (Λp) Scattering Parameters

With the elastic scattering in the final state significantly influencing physical observables — as it has already been noted in case of the energy dependence of the total cross section for hyperon production (fig. 4) — the effect of final state interaction has been used to extract low energy Λ–p scattering parameters [18]. With both unpolarized beam and unpolarized target, only spin averaged values for scattering length $\bar{a}$ and effective range $\bar{r}$ can be deduced from the data. However, the spin dependence is expected to be small [21, 22].

Compared to direct Λ–p scattering experiments, which are difficult to perform due to the short Λ lifetime, the complementary Λ–p final state interaction approach covers an energy range down to threshold, whereas direct data [19, 20] are available at excess energy values above 3.8 MeV (fig. 5).

An appropriate tool to study two–body correlations in a three–particle final state is provided by a Dalitz plot analysis depicting the double differential cross section

$$\frac{d^2\sigma}{dS_{pK}\, dS_{\Lambda K}} = \int f_C\left(q_{pK}\right)\ f_{FSI}\left(q_{\Lambda p}\right)\ d\rho^3, \qquad (2)$$

where S and q denote the two particle total energy and the momentum in the centre–of–mass of the respective subsystem. The s–wave ansatz in equation 2 assumes

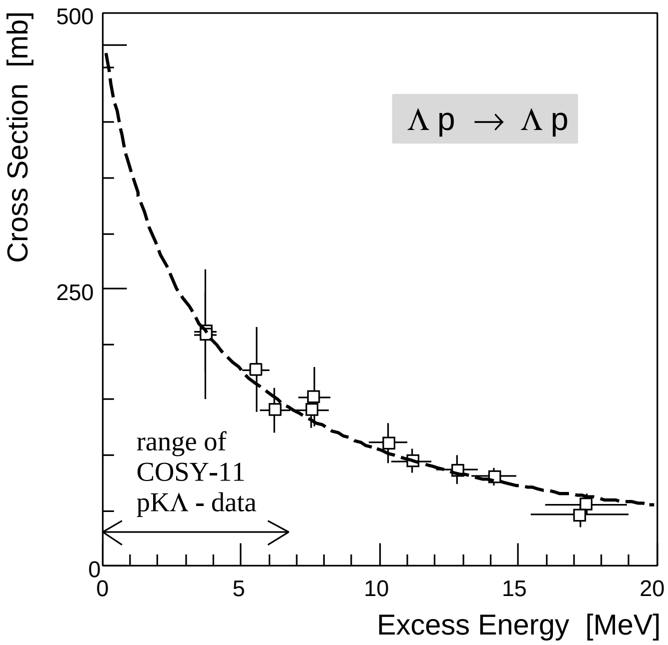

FIGURE 5. Total cross section for Λ–p elastic scattering close to threshold [19, 20]. The energy range of the COSY–11 data indicated by the arrow expands the range of available data down to threshold. A combined fit (dashed line) allows to determine spin averaged low energy Λ–p scattering parameters.

the production cross section to be dominated by the available three–body phase space volume $d\rho^3$ modified by variations from a uniform distribution due to the significant contributions to the final state interaction, i.e. the strong Λ–p interaction $f_{FSI}(q_{\Lambda p})$ and the p–K^+ Coulomb repulsion described by the Coulomb penetration factor $f_{coul}(q_{pK})$ [18, 23]. Parameterizing the attractive Λ–p interaction according to the Watson formalism [24]

$$f_{FSI}\left(q_{\Lambda p}\right) = \frac{1}{\bar{a}^2\, q^2 + \left(\frac{1}{2}\,\bar{r}\,\bar{a}\, q^2 - 1\right)^2} \tag{3}$$

the ansatz for the Dalitz plot contains only the spin averaged scattering length $\bar{a}$ and effective range $\bar{r}$ as free parameters, which significantly influence its differential occupation (fig. 6a). Monte Carlo generated Dalitz plot distributions for different values of scattering parameters $(\bar{a},\bar{r})$ folded with the acceptance of the detection system are compared to the experimental data (fig. 6b) with about 2400 events in total in a maximum likelihood fit.

In the analysis scattering parameters turn out to be strongly correlated constraining only the combination of scattering length and effective range in the $(\bar{a},\bar{r})$ plane

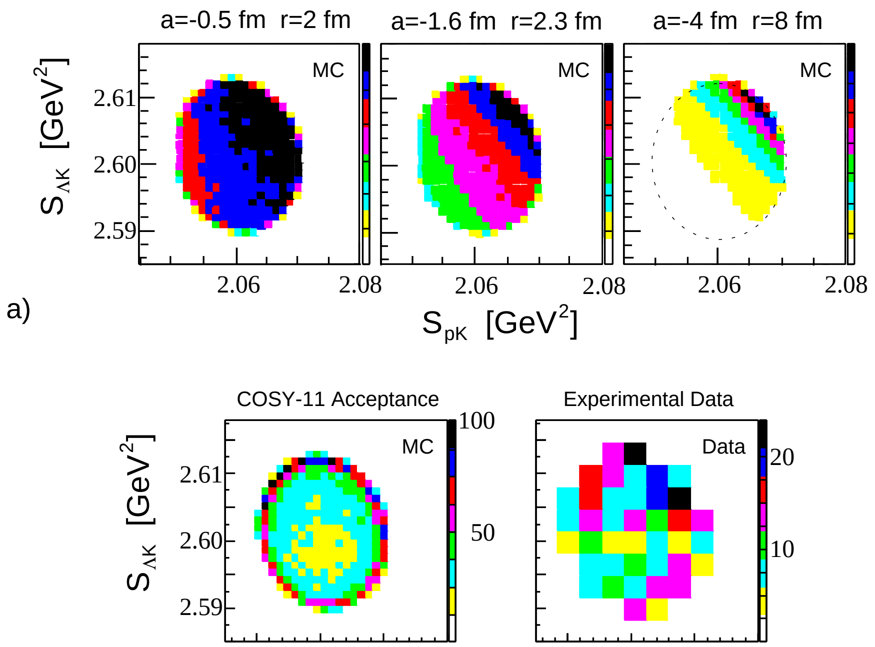

FIGURE 6. Dalitz plots for the reaction $pp \to pK^+\Lambda$ from a measurement at an excess energy of 7 MeV with respect to the $(pK^+\Lambda)$ threshold. Monte Carlo generated distributions demonstrate the sensitivity on low energy Λ–p scattering parameters (a). After being folded with the acceptance of the detection system, the distributions are compared to the experimental data covering the complete kinematically allowed range (b).

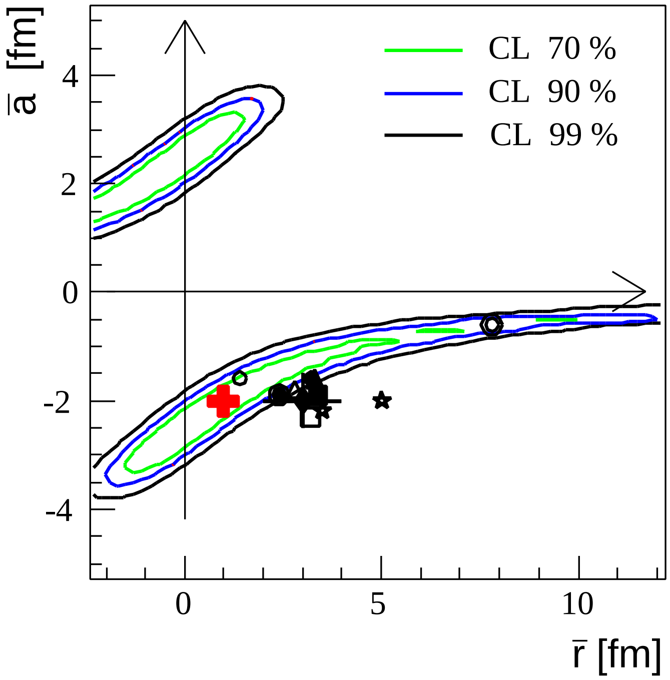

FIGURE 7. Constraints on low energy Λ–p scattering parameters from the logarithm of a likelihood function in the ($\bar{a}$,$\bar{r}$) plane based on close–to–threshold COSY–11 data. Unphysical solutions with a positive scattering length implying a (Λp) bound state are to be excluded. In comparison, available literature values [13,19–22,25] are included. A combined fit with Λ–p elastic scattering data results in spin averaged values of $\bar{a} = -2.0\,\mathrm{fm}$ and $\bar{r} = 1.0\,\mathrm{fm}$ for the Λ–p scattering length and effective range, respectively, as indicated by the filled cross.

(fig. 7). In comparison, available experimental and theoretical values [13, 19–22, 25] are located close but for the most part slightly outside the 99 % confidence level contour.

Separate values of scattering length and effective range are accessible using the complementary additional experimental information from low energy Λ–p elastic scattering [19, 20]. A fit of the elastic cross section parameterized in terms of the scattering parameters is constrained according to the maximum likelihood ridge from the COSY–11 data (fig. 5). Although due to the strong correlation of the parameters errors are difficult to derive, the combined fit allows a new determination of spin–averaged Λ–p scattering parameters (fig. 7)

$$\bar{a}_{\Lambda p} = -2.0\,\mathrm{fm},\ \bar{r}_{\Lambda p} = 1.0\,\mathrm{fm}. \tag{4}$$

ELEMENTARY ANTIKAON PRODUCTION

Studies of $K\overline{K}$ production have been motivated originally by the ongoing discussions on the nature of the scalar objects $f_0\,(980)$ and $a_0\,(980)$ [26–29]. Within the framework of the Jülich meson exchange model [29] a $K\overline{K}$ molecule structure of the $f_0\,(980)$ is closely related to the strength of the $K\overline{K}$ interaction, which determines both shape and absolute value of the $\pi\pi \rightarrow K\overline{K}$ transitions [30]. Similar effects in $K\overline{K}$ production in proton–proton scattering should probe the $K\overline{K}$ interaction and thus a possible $K\overline{K}$ nature of the $f_0\,(980)$.

At present, the experimental approach falls short of its initial objective, due to unexpectedly low cross sections and, consequently, low statistics. However, despite the vicinity of comparatively broad hyperon resonances, preliminary data show clear signals of the elementary antikaon production.

Event Selection and Preliminary Results

Analogously to the experimental technique described in case of the hyperon production channels, (ppK^+) final states are identified from two protons and an additionally identified kaon using the indirect time–of–flight method.

First data showed a large scattering of events on the scale of the missing mass in the order of $50\,\mathrm{MeV/c^2}$ with respect to the identified (ppK^+) subsystem [31] contrasting sharply with typical values known from hyperon production at COSY–11 (fig. 3). However, with no detection of a negatively charged kaon being required,

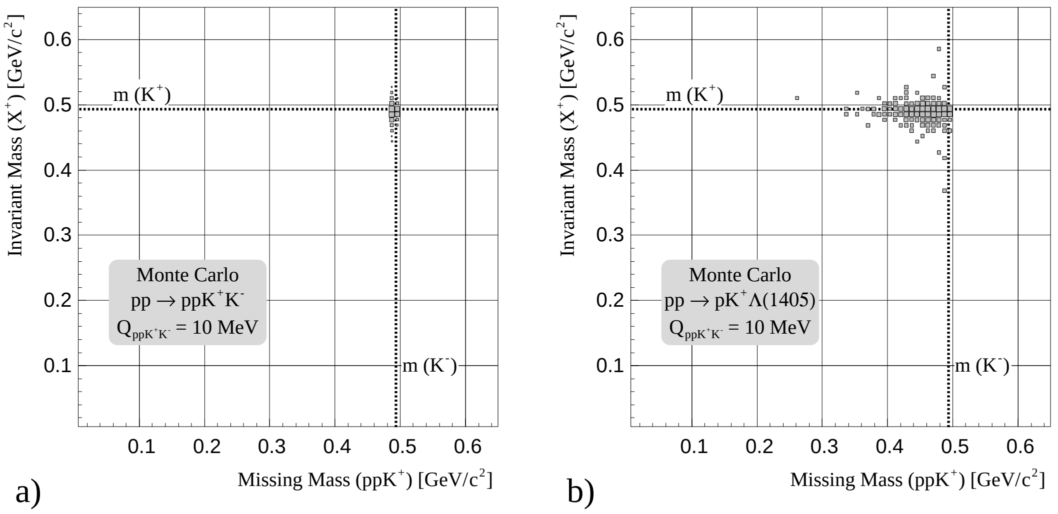

FIGURE 8. Invariant mass of a third positively charged ejectile in addition to two identified protons versus missing mass with respect to the assumed (ppK^+)–subsystem at an excess energy of $10\,\mathrm{MeV}$ above the (K^+K^-) threshold for the reactions $pp \rightarrow ppK^+K^-$ (a) and $pp \rightarrow pK^+\Lambda\,(1405)$ (b) from Monte Carlo simulations.

the reaction type pp $\rightarrow$ ppK$^+$X, with X denoting an undetected negatively charged meson system, remains ambiguous concerning the underlying reaction mechanism: One of the identified protons may originate from the weak decay of an initially produced hyperon via pp $\rightarrow$ pK$^+$Y $\rightarrow$ pK$^+$pX. A dominant influence of the hyperon resonances $\Lambda\,(1405)$ and $\Sigma\,(1385)$ is expected due to an acceptance of the detection system decreasing with increasing excess energy. In consequence, the missing mass with respect to the identified (ppK$^+$) system may shift to values too low for a (ppK$^+$K$^-$) hypothesis as demonstrated by the simulations in figure 8, which give a strong hint on the importance of hyperon resonance channels in view of the large scattering with respect to the (ppK$^+$) missing mass observed in the data (see also fig. 9).

¿From the above discussion, to discriminate the (ppK$^+$K$^-$) final state from hyperon production channels, the K$^-$ identification seems to be experimentally crucial. Preliminary results from data taken at an excess energy of 17.1 MeV with respect to the (ppK$^+$K$^-$) threshold and at a significantly increased integrated luminosity in September 1998 are presented in figure 9a [32]. For events within the experimental resolutions for the charged kaon mass on both the scale of the invariant mass of a third charged ejectile and the missing mass of the assumed (ppK$^+$) subsystem a K$^-$ consistent hit in the negative particle detection system is required: ¿From the measured momenta of positively charged ejectiles and momentum conservation the K$^-$ momentum is calculated. Thus, the negatively charged

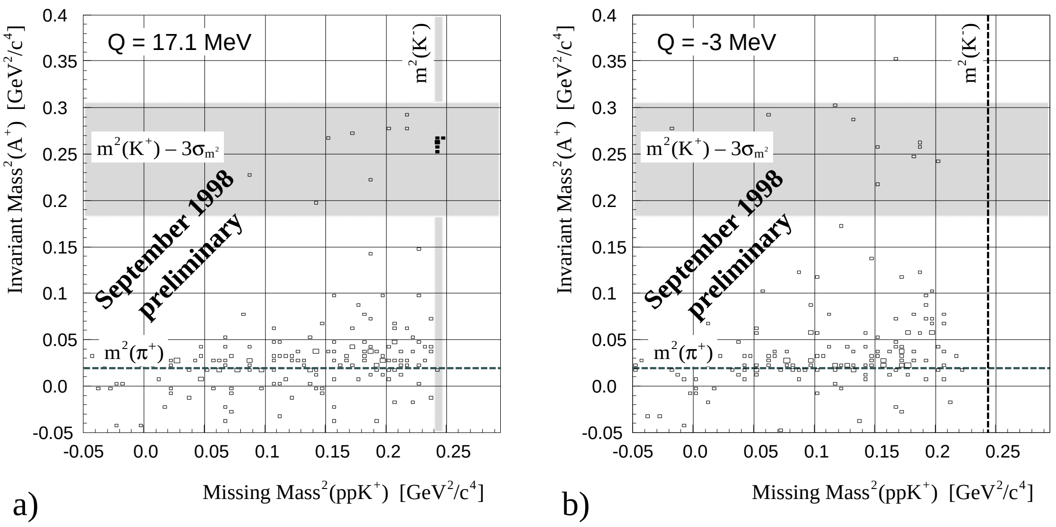

FIGURE 9. Preliminary results for the invariant mass of a third positively charged ejectile in addition to two identified protons versus the missing mass with respect to the assumed (ppK$^+$)–subsystem at an excess energy of 17.1 MeV above (a) and -3 MeV (b) below the (K$^+$K$^-$) threshold, respectively. Experimental resolutions corresponding to three standard deviations are indicated by the shaded regions. For events within the limits of both the invariant mass and missing mass resolutions a K$^-$ consistent hit in the negative particle detection system is required [32].

kaon can be traced through the dipole field to the dedicated detection system and the reconstructed hit position is compared to the registered signals in both silicon pad detector and scintillator. Within the resolution for the invariant mass of the assumed positively charged kaon a group of six events clearly stands out at a missing mass corresponding to the K^- mass. In a measurement below threshold (fig. 9b) at a comparable value of the integrated luminosity the region expected for a (ppK^+K^-) final state remains completely empty.

To confirm this result corresponding to a first preliminary cross section value for K^+K^- production in the order slightly below 1 nb, additional data have been taken at the same excess energy of 17.1 MeV in 1999. Figure 10 depicts a very preliminary result for the missing mass with respect to an identified (ppK^+) subsystem at a further increased luminosity from an increase in beam intensity [32]: In the missing mass spectrum both a broad structure in agreement with expectations for a $pK^+\Sigma\,(1385)\,/\Lambda\,(1405)$ final state and a clearly separated distinct signal corresponding to a (ppK^+K^-) hypothesis are visible.

In conclusion, strong experimental evidence is deduced from the data for an exclusive identification of the elementary antikaon production channel in proton–proton scattering. Final values of the total cross section will be available in the near future.

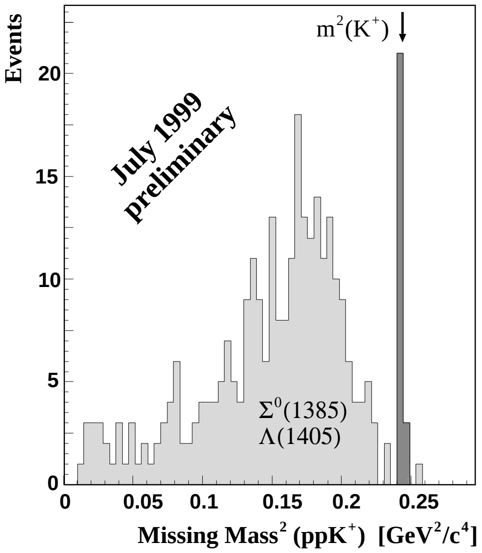

FIGURE 10. Missing mass with respect to an identified (ppK^+)–subsystem at an excess energy of 17.1 MeV above the (K^+K^-) threshold from July 1999 (very preliminary [32]).

FROM PRESENT TO FUTURE

Besides the production of isoscalar (η, η', see also [33]) and vector mesons (ω, Φ), both kaon and antikaon production channels in proton–proton scattering will be part of the experimental programme at the COSY–11 facility in future.

The strong suppression of the Σ^0 signal close to threshold observed in the exclusive pp $\rightarrow$ p$K^+\Lambda/\Sigma^0$ measurements as compared to the ratio at high energies might be explained by a destructive interference of kaon and pion exchange. A measurement of the energy dependence of the production ratio both at COSY–11 and the complementary TOF spectrometer at COSY [34] will further constrain the interpretation of the close–to–threshold data. An extension of the COSY–11 detection system by a dedicated Cerenkov detector for a unique kaon identification independent of the indirect time–of–flight method will provide access to final states of different isospin configuration, i.e. the pp $\rightarrow$ n$K^+\Sigma^+$ channel.

Strong experimental evidence for an exclusive identification of the elementary antikaon production channel in the nucleon–nucleon interaction — the (ppK^+K^-) final state — will lead to a first total cross section value in the near future. The use of additional drift chambers at the exit window of the momentum analyzing dipole will further increase the acceptance for K^+ detection by a factor of two. Thus, already at present luminosity values, a determination of the close–to–threshold excitation function for K^+K^- production is feasible.

ACKNOWLEDGEMENTS

The COSY–11 collaboration is grateful to numerous people who have supported the experimental facility. The COSY operating team significantly contributed to the presented results by providing the excellent quality proton beam. Explicitly, we would like to thank J. Haidenbauer, C. Hanhart and C. Wilkin for many fruitful discussions.

REFERENCES

1. Maier, R., *Nucl. Instr. & Meth.* **A 390** 1–8 (1997) and Maier, R., *Nucl. Phys. News Int.* **7** No. 4 5–13 (1997).
2. Dombrowski, H. et al., *Nucl. Instr. & Meth.* **A 386** 228–234 (1997).
3. Brauksiepe, S. et al., *Nucl. Instr. & Meth.* **A 376** 397–410 (1996).
4. Albers, D. et al., *Phys. Rev. Lett.* **78** 1652–1655 (1997)
5. Balewski, J.T. et al., *Phys. Lett.* **B 388** 859–865 (1996).
6. Balewski, J.T. et al., *Phys. Lett.* **B 420** 211–216 (1998).
7. Sewerin, S., Schepers, G. et al., *Phys. Rev. Lett.* **83** 682–685 (1999).
8. Fäldt, G. and Wilkin, C., *Z. Phys.* **A 357** 241–243 (1997).
9. Flaminio, V., Moorhead, W.G., Morrison, D.R.O. and Rivoire, N., *Compilation of Cross Sections*, CERN–HERA 84–01 (1984).

10. Jones, J. et al., *Phys. Rev. Lett.* **26** 860–863 (1972); Baker, R.D. et al., *Nucl. Phys.* **B 145** 402–408 (1978); Saxon, D.H. et al., *Nucl. Phys.* **B 162** 522–546 (1980); Hart, J.C. et al., *Nucl. Phys.* **B 166** 73–83 (1980); Candlin, D.J. et al., *Nucl. Phys.* **B 226** 1–28 (1983); Candlin, D.J. et al., *Nucl. Phys.* **B 311** 613–629 (1988).
11. De Swart, J.J., *Rev. Mod. Phys.* **35** 916–939 (1963); Dover, C.B. and Gal., A., *Prog. Part. Nucl. Phys.* **12** 171–239 (1985).
12. Siebert, R. et al., *Nucl. Phys.* **A 567** 819–843 (1994).
13. Tan, T.H., *Phys. Rev. Lett.* **23** 395–398 (1969).
14. Gasparian, A., Haidenbauer, J., Hanhart, C., Kondratyuk, L. and Speth, J., e–Print Archive nucl-th/9909017 (1999) and proceedings of this conference.
15. Tsushima, K., Sibirtsev, A. and Thomas, A.W., *Phys. Lett.* **B 390** 29–35 (1997).
16. Tsushima, K., Sibirtsev, A., Thomas, A.W. and Li, G.Q., *Phys. Rev.* **C 59** 369–387 (1999).
17. Kaiser, N., *Eur. Phys. J.* **A 5** 105–110 (1999).
18. Balewski, J.T. et al., *Eur. Phys. J.* **A 2** 99–104 (1998).
19. Alexander, G. et al., *Phys. Rev.* **173** 1452–1460 (1968).
20. Sechi–Zorn, B. et al., *Phys. Rev.* **175** 1735–1740 (1968).
21. Holzenkamp, B., Holinde, K. and Speth, J., *Nucl. Phys.* **A 500** 485–528 (1989); Reuber, A., Holinde, K. and Speth, J., *Nucl. Phys.* **A 570** 543–579 (1994).
22. Nagels, M.M., Rijken, T.A. and de Swart, J.J., *Phys. Rev.* **D 20** 1633–1645 (1979).
23. Hanhart, C. et al., *Phys. Lett.* **B 358** 21–26 (1995).
24. Goldberger, M.L. and Watson, K.M., *Collision Theory*, New York: John Wiley & Sons, 1964.
25. Maessen, P.M.M., Rijken, T.A. and de Swart, J.J., *Phys. Rev.* **C 40** 2226–2245 (1989).
26. Jaffe, R.L., *Phys. Rev.* **D 15** 267–280 (1977).
27. Weinstein, J. and Isgur, N., *Phys. Rev.* **D 41** 2236–2257 (1990).
28. Morgan, D. and Pennington, M.R., *Phys. Rev.* **D 48** 1185–1204 (1993).
29. Lohse, D., Durso, J.W., Holinde, K. and Speth, J., *Nucl. Phys.* **A 516** 513–548 (1990).
30. Krehl, O., Rapp, R. and Speth, J., *Phys. Lett.* **B 390** 23–28 (1997).
31. Lister, T., PhD thesis: Westfälische Wilhelms–Universität Münster, 1998; Lister, T., Quentmeier, C. and Wolke, M., *Annual Report 1998 IKP/COSY*: Forschungszentrum Jülich, Jül–3640, 1999.
32. Quentmeier, C., PhD thesis: Westfälische Wilhelms–Unisversität Münster, in preparation.
33. Moskal, P. et al., proceedings of this conference.
34. Wirth, S. et al., proceedings of this conference.